Analyst

Cite this: *Analyst*, 2012, **137**, 370

www.rsc.org/analyst

PAPER

Experimental investigation of beam heating in a soft X-ray scanning transmission X-ray microscope

Adam F. G. Leontowich* and Adam P. Hitchcock

Received 7th July 2011, Accepted 29th October 2011
DOI: 10.1039/c1an15688h

A variable temperature sample holder with an operational range of 15 to 200 °C and an accuracy of ±1 °C has been fabricated for scanning transmission X-ray microscopes (STXM). Here we describe the device, and use it to image the polycrystalline morphology of solid stearic acid and palmitic acid at temperatures near their respective melting points as a means of checking for possible sample heating caused by the focused X-ray beam. The melting points observed in STXM were identical to those observed by conventional methods within measurement uncertainty, even under the most extreme, high dose rate imaging conditions investigated. The beam-induced temperature rise in the sample is inferred to be below 1 °C for dose rates of up to 2.7 GGy/s.

Introduction

Improvements in the manufacture of Fresnel zone plate lenses[1,2] enable the current generation of soft X-ray (60–2500 eV) scanning transmission X-ray microscopes (STXM) to focus as much as 10^8 photons/s into a spot of continuously decreasing diameter. The size of the spot produced at the focal plane of a zone plate is proportional to the width of it's outermost zone,[3] which for this study is 25 nm. Assuming that the zone plate is manufactured within certain tolerances,[4] free of aberrations (which may not always be the case[5]), and the beamline and STXM are tuned to produce the conditions necessary for diffraction-limited focusing[4–6] (routine with current designs and components[7–12]) 83.8% of the radiation diffracted into the first order focal point ends up inside a circle (the Airy disk) with a diameter of 61 nm at the focal plane.[13] The net result is that, with typical microscope settings, the sample will absorb energy at a rate on the order of 0.1–1 GGy/s. By opening the monochromator entrance and/or exit slits, it is possible to exceed 3 GGy/s. However, this is accompanied by a reduction in spatial and energy resolution, and could exceed the limit of linearity of the detector.

The amount of energy absorbed by the sample during STXM investigation has been hypothesized to induce a rise in sample temperature (T), which could affect the outcomes of experiments in a variety of ways. (i) The heat generated could directly alter the sample. Braun *et al.*[14] observed alteration of polymer and soot extract samples exposed to the focused X-ray beam and attributed it to heat dissipation in the sample, though no data to support this claim appears in their report and it is not clear how this effect was separated from other radiation-induced damage mechanisms.[15–17] (ii) Fu *et al.*[18] entertained the possibility that a beam-induced rise in T could be large enough to cause reorientation of ordered alkane chains, introducing uncertainty in quantifying polarization dependent signals. (iii) Beam-induced heating could indirectly alter the sample. X-rays can create reactive molecular fragments such as radicals or ions in the sample,[19–21] and migration of such molecular fragments is known to be T dependent.[22] Wang *et al.*[23] considered the possibility of beam-induced heating affecting the migration distance of radicals/ions in thin polymer layers, but then negated it by calculating the rise in T to be less than 1 °C under their conditions. (iv) A rise in T could affect the quality of spectroscopic data. Certain X-ray absorption spectral features change shape for T changes in the range of tens of °C. Such changes have been shown to be reversible and not due to radiation damage.[24] An experimental determination of beam-induced sample heating deconvoluted from other radiation-induced effects would be a welcome compliment to the calculation of Wang *et al.*[23] However it is not a trivial task to accurately measure a T change within a sub-100 nm diameter area. To our knowledge there has not been an experimental study of beam-induced sample heating in STXM.

In the work reported here we sought to determine *via* experiment whether or not significant beam-induced sample heating occurs over STXM imaging conditions ranging from typical to extreme, using an indirect method inspired by reports from the early days of electron microscopy (reviewed by Reimer and Christenhusz[25]). The polycrystalline morphology of thin films (30–200 nm) of fatty acids was imaged by STXM as a function of T. To perform this experiment a variable T sample holder device which employs a Peltier element was constructed. Here the device is described and the accuracy of the control of sample T is evaluated. The T values at which the fatty acids undergo a solid to liquid phase transition were recorded while being imaged at soft X-ray photon energies in STXM, and compared to values

Brockhouse Institute for Materials Research, McMaster University, 1280 Main St. W. L8S 4M1, Hamilton, Canada. E-mail: leontoaf@mcmaster.ca; Fax: +1 905.521.2773; Tel: +1 905.525.9140 x24864

obtained by a conventional melting point (mp) apparatus. Under the most extreme STXM imaging conditions noted, beam-induced sample heating is shown to be practically negligible – an upper limit of 1 °C is estimated.

Experimental

Variable temperature sample holder device

The device fabricated to enable this experiment is presented in Fig. 1. It was designed to fit the existing three pin kinematic sample mount of Advanced Light Source (ALS) STXM 5.3.2.2[8] (formerly referred to as 5.3.2), at Lawrence Berkeley National Labs (LBNL) without modification so as to minimize installation time. The device fits the sample mounts of all operational STXMs to date which are based on the ALS 5.3.2.2 design (ALS 11.0.2,[9] Canadian Light Source (CLS) 10ID-1,[10] Swiss Light Source X07DA,[11] BESSY II UE46[12]) without additional modification. The device holds samples in X, Y and Z positions that are within tens of μm of a standard sample holder, which was not a trivial feat considering the spatial constraints. When operated in focus at 280 eV the distances from the sample to the zone plate, order sorting aperture and detector are 1355 μm, 280 μm and ~2 mm, respectively. The bottom part of the device, which holds up to three samples, is thermally isolated from the rest of the device. Its T is monitored by a K type thermocouple, read to 1 °C (DM6802B, Sampo). Heating and cooling is enabled by a Peltier thermoelectric element (TE-65-0.6-0.8, TE Technology, Inc.) controlled with a variable DC power supply (GPS-1850D, GW Instek). In this configuration, the bottom part of the device has a T range of 15 to 200 °C.

Sample preparation

Stearic acid (99%, Simga-Aldrich) was purified by multiple recrystallizations from hot 4-methyl-2-pentanone (>98.5% ACS reagent grade, Sigma-Aldrich), and was pure by ^{1}H NMR (600 MHz, AV 600, Bruker), mp 69.8 °C. Palmitic acid (99%, Simga-Aldrich) was used as received, mp 62.7 °C. These mp values were determined using a conventional mp apparatus (MF370, Gallenkamp). 75 nm Si_3N_4 windows (1 mm × 1 mm window area in a 5 mm × 5 mm Si wafer frame) were purchased from Norcada Inc.

All samples investigated were prepared in the following manner: A very small (sub-mg) amount of stearic acid or palmitic acid was deposited onto the flat side of a Si_3N_4 window, which rested on the device. The T was raised until the solid melted, forming a small drop. With the T held above the mp, a second Si_3N_4 window was overlaid (flat side down) onto the drop, confining it between the two windows. The T was then slowly reduced to room T, and the thin liquid film solidified, a process readily observable if the sample is prepared under an optical microscope. Finally, the sample was affixed to the device with two small dabs of epoxy. Fatty acid film thicknesses, which were determined to be 30–200 nm by near edge X-ray absorption fine structure (NEXAFS) spectroscopy, are typical of most STXM samples and within the range acceptable for soft X-ray NEXAFS measurements free of absorption saturation.

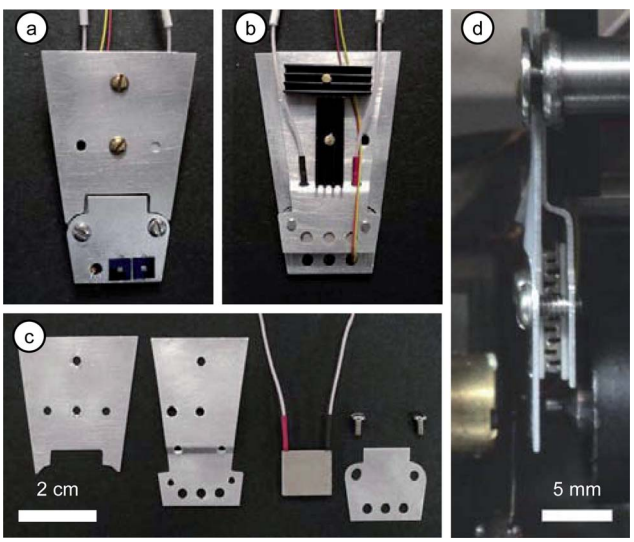

Fig. 1 a) Front view of the variable temperature sample holder device, assembled, with two samples affixed. b) Back view, assembled. c) Front view, disassembled. d) Side view, mounted in ALS STXM 5.3.2.2 with zone plate, order sorting aperture and detector distances tuned for O 1s edge measurements.

Microscopy

In STXM, monochromatic X-rays are focused down to a small focal point. Samples are positioned at the focal plane and X-Y raster scanned through this focused probe while the transmitted photon flux is simultaneously recorded to form transmission images at X-ray photon energies. These transmission images can then be converted to optical density (OD) images using the Lambert-Beer law,

$$OD = -\ln(I/I_0) = \mu \cdot \rho \cdot t \quad (1)$$

where I_0 is the incident photon flux, I is the transmitted photon flux for each pixel of the image, μ is the mass absorption coefficient, ρ is density, and t is sample thickness. In a second mode of operation, X-ray transmission spectra can be acquired by positioning the sample at or near the focal plane and scanning the monochromator across a photon energy range of interest while recording I. The X-ray transmission spectra can be converted to X-ray absorption spectra by collecting an I_0 spectrum and applying the above relationship. Several excellent descriptions of STXM exist elsewhere.[15,26]

STXM measurements at C 1s (K) edge photon energies were performed using ALS STXM 5.3.2.2,[8] while those at the O 1s edge were performed using CLS STXM 10ID-1.[10] Both microscopes use zone plate lenses with identical parameters (25 nm outermost zonewidth, 240 μm diameter, 90 μm central stop) supplied by the Center for X-ray Optics (CXRO), LBNL. All measurements were carried out with the STXM enclosure backfilled with He to 250 Torr, after evacuation of air. A N_2 gas filter (1 m path at a pressure of 0.6 Torr) was used to suppress second order radiation from the monochromator for measurements performed at the C 1s edge. The efficiency of the scintillation-photo multiplier tube (PMT) detector at the C and O 1s edge regions,[8] and other instrumental parameters have been taken into account in computing the absorbed dose rates

presented, which are believed to be precise within 10% using methods described in detail earlier.[17,23] Optical microscope images were obtained with an Olympus BX51 optical microscope equipped with a polarizer–analyzer set and a CCD camera, operating in transmission mode.

Results

Device accuracy

Optical microscope and STXM OD images of a stearic acid sample at 25 °C are presented in Fig. 2. Fig. 2a is an optical microscope image of the entire sample. Fig. 2b is an OD image at 320 eV of a select area. At 320 eV, away from the fine structure of the absorption edge, C 1s X-ray absorption cross sections become atomic-like;[27] for a pure material, a change in contrast in an OD image at this energy indicates a change in thickness and/or density (eqn. (1)). Overall there is a significant increase in absorption going from the top of the OD image to the bottom. In addition, the contrast is not uniform; fine heterogeneous contrast fluctuations (±5% variations in OD) are observed. Fig. 2c is a polarized (analyser orthogonal to polarizer) optical microscope image of the same area. A heterogenerous contrast pattern is observed, identical to that observed by STXM. The contrast in Fig. 2c is due to birefringence; areas which show increased contrast are ordered along certain directions. Polarized optical microscope images of fatty acid samples in the liquid state showed zero contrast. Therefore, since identical heterogeneous contrast patterns are observed by STXM and polarized optical microscopy, we ascribe the heterogeneous contrast patterns observed in the STXM OD images of the solid fatty acid samples to be primarily due to fatty acid film thickness variations arising from the way crystal domains of different orientation are organized spatially.

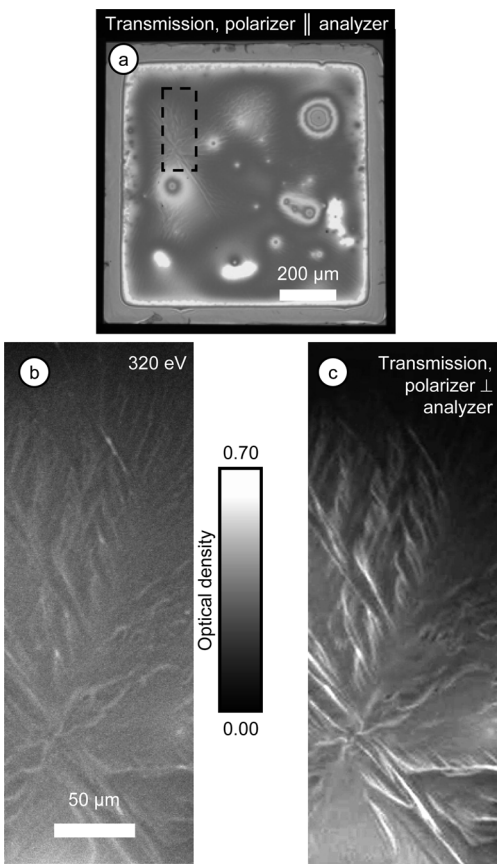

Fig. 2 a) Optical microscope image of stearic acid confined between two Si_3N_4 windows. b) STXM optical density (OD) image, 320 eV, of the area outlined by the dotted line in a). c) Polarized optical microscope image of the area outlined by the dotted line in a).

To determine the accuracy of T-control and T-measurement of the device, a stearic acid sample was affixed to the device and observed under the optical microscope while heating. The polarized optical microscope image was continuously monitored while T was raised at a rate of approximately 4 °C min^{-1}. Some signs of melting, notably movement of the solid material and some disappearance of contrast in the image, were observed at 67 °C. This low onset may be due to possible impurities on the Si_3N_4 windows. The contrast in the image completely and rapidly disappeared when T = 70 °C and was consistent across the whole 1 mm × 1 mm sample. In summary, the stearic acid sample mounted on the device melted at the identical T (within measurement uncertainty) determined earlier for the same material by a mp apparatus. Therefore the control system and temperature measurement of the device are accurate within ±1 °C. Note that T is measured at the bottom part of the device to which the samples are affixed, not the samples themselves. We therefore infer that the thin fatty acid films and the Si_3N_4 windows conduct heat sufficiently well and evenly enough that the samples are in thermal equilibrium with the device, at these conditions.

Measurement of beam-induced heating in STXM

A palmitic acid sample was affixed to the device and mounted in ALS STXM 5.3.2.2. The sample was imaged at 288.0 eV with an entrance slit setting of 50 μm, exit slit settings of 25 μm × 25 μm, and a pixel dwell time of 2 ms. These settings are typical for diffraction-limited imaging at the C 1s edge. The dose rate was calculated to be 360 ± 40 MGy/s. A series of OD images of the same area of this sample at various T's are presented in Fig. 3. In Fig. 3a, acquired at a constant T of 25 °C, solid palmitic acid fills the majority of the imaged area, except for the area along the right side of the image which is free of material (OD = 0.00). The solid shows heterogeneous contrast as discussed previously. After this image was acquired sample T was elevated to 58 °C. T was gradually increased from 58 to 65 °C as the next image (Fig. 3b) was acquired (STXM images are acquired one line at a time; the acquisition/scan direction was always from bottom to top). Compared to the image acquired at constant T = 25 °C (Fig. 3a), details in the image began to change when T = 61 °C. As the scan progressed further, the areas that previously showed heterogeneous contrast took on a smooth, homogeneous appearance when T = 63 °C and above. This suggests that for the remainder of the image acquisition the palmitic acid was in the liquid state, which would be expected at this T. T = 65 °C was maintained after this image (Fig. 3b) had been acquired, and another image of the same area was recorded at constant T = 65 °C (Fig. 3c). The palmitic acid in this smooth featureless image is unambiguously in the liquid state. The area on the right of this image, which in the solid state (Fig. 3a) had an OD = 0.00, now

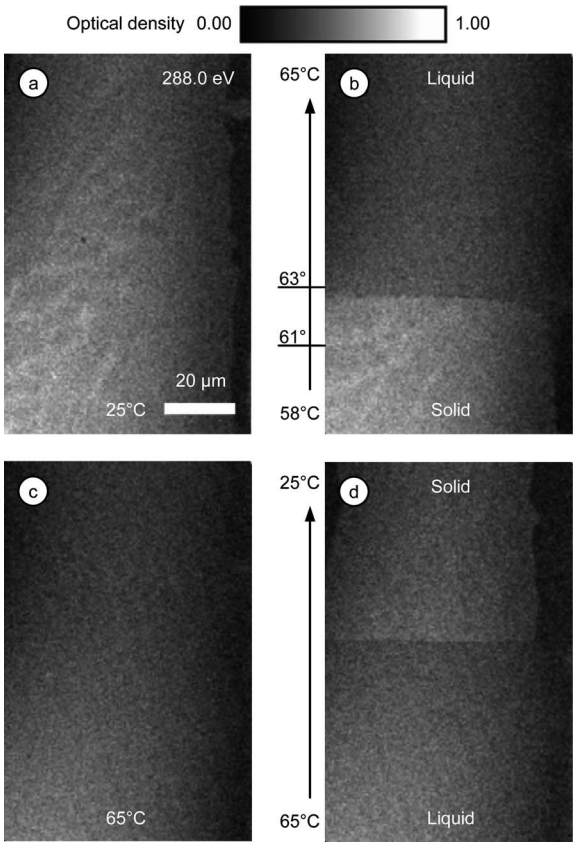

Fig. 3 STXM OD images, 288.0 eV, of palmitic acid confined between two Si_3N_4 windows at various temperatures. a) Solid at 25 °C. b) On raising the temperature throughout the image acquisition from 58 to 65 °C, the heterogeneous contrast characteristic of the solid began to distort at 61 °C. Contrast became homogenous at 63 °C. c) Liquid at 65 °C. d) Rapid cooling during image acquisition. All images are same position and OD scale.

has an OD of ~0.05, indicating movement of material *i.e.* flow into this area. Comparing Fig. 3a and 3c, a change in thickness of the material occurred, which is ascribed to the flow of liquid between the confines of the two Si_3N_4 windows. Sample T was rapidly decreased from 65 to 25 °C as a final image was acquired (Fig. 3d). Midway through this image acquisition defined features reappeared, which we infer as the point at which the liquid palmitic acid had solidified. At this point the edge observed in Fig. 3a also reappeared as the material contracts upon solidifying. The palmitic acid is in the solid state for the remainder of the image acquistion.

In a second experiment, a stearic acid sample was affixed to the device and mounted in CLS STXM 10ID-1. An O 1s NEXAFS spectrum was recorded at 25 °C and is presented in Fig. 4. Based on this spectrum, we chose to perform our T-dependent imaging experiment at 532.2 eV as it is the photon energy of maximum absorption at the O 1s edge for this molecule. The exit slit settings (15 μm × 15 μm) were chosen such that the photon flux (I_0) was just below the ~20 MHz limit of linearity of the scintillation-PMT detector.[8] The dose rate was calculated to be 2670 ± 160 MGy/s. These conditions, which are rarely used due to the high dose rate, represent our attempt to create the most extreme imaging conditions which might be encountered in a STXM (see

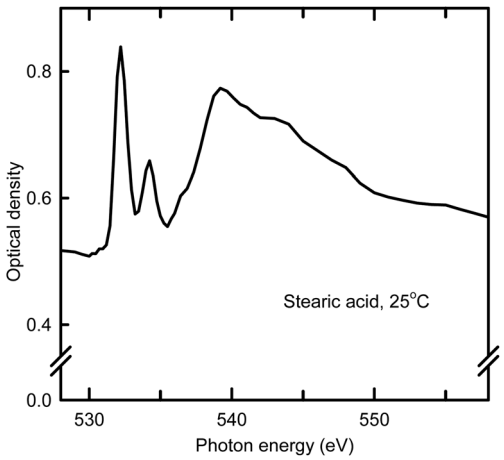

Fig. 4 NEXAFS spectrum of stearic acid at 25 °C, in the region of the O 1s edge.

further comments in the discussion). A series of OD images of the same area of this sample at various T's are presented in Fig. 5. The image in Fig. 5a was acquired with the stearic acid in the solid phase at a constant T = 25 °C. After this image was acquired sample T was elevated to 59 °C (10 °C below the mp). The next image (Fig. 5b) was acquired at a constant T = 59 °C. The heterogeneous contrast pattern in Fig. 5a and 5b is clearly identical. T was gradually increased from 59 to 70 °C as another image of the same area (Fig. 5c) was acquired. The heterogeneous contrast pattern showed signs of distortion at 67 °C, and by 70 °C the contrast in the image became homogenous. T was reduced from 70 to 50 °C as another image (Fig. 5d) was acquired of the same area. Heterogeneous contrast returned as the stearic acid solidified. The solid material took on a new heterogeneous contrast pattern, different from that of the same area before the melt-freeze cycle. The image presented in Fig. 5e was acquired at a constant T = 25 °C to record the new contrast pattern.

Discussion

All observations regarding the effects of T on the polycrystalline morphology of thin fatty acid films noted in the results section can also be made under the polarized optical microscope on the lab bench, and should not come as a surprise. However, these observations when made with a STXM reveal useful information about beam-induced sample heating. The fatty acid samples absorbed energy from the soft X-ray imaging process while the T was raised through their respective melting points using a variable temperature sample holder device. If this additional energy induced a significant rise in sample T, one would expect melting to occur at a T below the conventionally determined mps. This was not observed. Both palmitic acid and stearic acid were observed to melt at T values identical to those obtained with a conventional mp apparatus within measurement uncertainty while simultaneously being imaged with STXM (which could now be considered as a very expensive mp apparatus!). Upon transitioning from solid to liquid to solid, the heterogeneous contrast patterns of solid fatty acid films change randomly (Fig. 5). If, during imaging, the beam had induced a rise in T sufficient to melt the sample, the heterogeneous contrast pattern

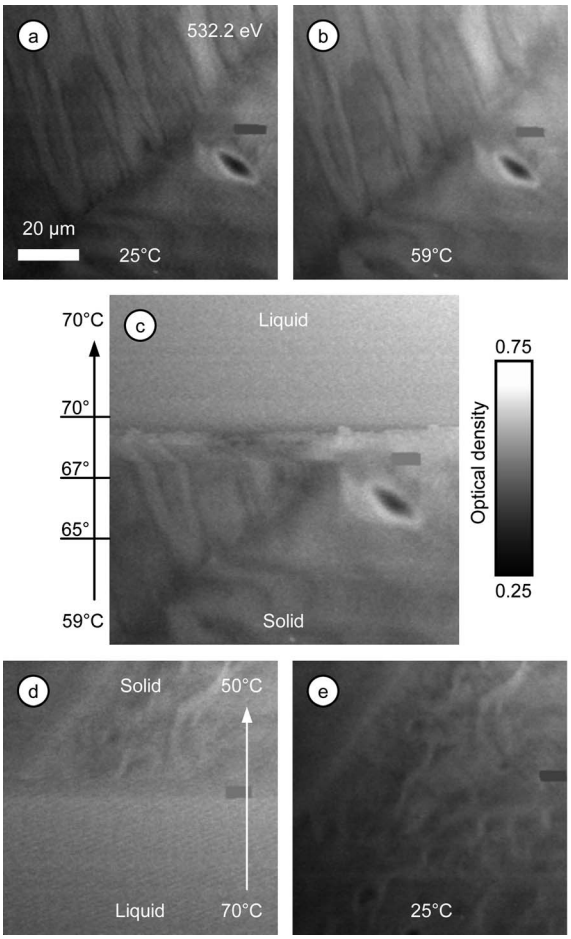

Fig. 5 STXM OD images, 532.2 eV, of stearic acid confined between two Si_3N_4 windows at various temperatures. a) Solid at 25 °C. b) Solid at 59 °C. c) On raising the temperature throughout the image acquisition from 59 to 70 °C, the image began to distort at 67 °C. Contrast became homogenous at 70 °C. d) Slow cooling during image acquistion. e) New crystalline pattern which formed after solidifying, 25 °C. All images are same position and OD scale. The grey rectangle in each image covers an extremely dense speck of material which has been omitted so that the contrast of the sample is enhanced.

of the imaged area would change upon successive imaging. However, successive images of the same area of the sample made at 25 °C and at a few °C below the mp were identical, again negating a significant beam-induced rise in sample T. Note that in our analysis we have ignored possible additional thermal contributions from X-ray absorption by the two 75 nm Si_3N_4 windows which encapsulate the fatty acids. Although they are sufficiently transparent for imaging with soft X-rays, each attenuates the flux by 30–35% throughout the C 1s edge region, and 40–45% throughout the O 1s edge region. The heat generated at the focal spot within these windows is also conducted to the sample, yet the T rise of the material within the focal spot is negligible.

Photon flux rates above 20 MHz, greater than the limit of linearity of the scintillation-PMT detector, can be achieved by further opening the monochromator entrance and/or exit slits, especially for those STXMs on undulator beamlines such as CLS 10ID-1. Flux rates above 20 MHz can be quantified. However, it would be unusual for a STXM equipped with a scintillation-PMT detector (at present, the most commonly used detector) to be operated in the non-linear high dose rate range for making images and collecting NEXAFS spectra. Other detectors/methods of detection have been used for this high photon flux regime, such as photodiodes,[28] avalanche photodiodes,[12] channeltrons,[29] monitoring sample current (conductive samples only),[30] or fluorescence.[31] One must also consider that if the slits are opened too wide, the zone plate focusing may no longer be diffraction-limited, causing the spot diameter to increase *i.e.* the dose rate will no longer be linearly proportional to the flux rate. In this investigation we have restricted our determination of the beam-induced rise in sample T to those conditions encountered in the vast majority of STXM investigations past and present, which we define as collecting images and NEXAFS spectra with the microscope set for diffraction-limited focusing conditions, in transmission mode with a scintillation-PMT detector, operating within the limit of linearity of the detector. The O 1s experiments were performed at an absorbed dose rate of 2670 ± 160 MGy/s, the maximum possible under linear photon counting conditions using the scintillation-PMT detector. No sign of beam-induced sample heating was found. Therefore it is inferred that any beam-induced rise in sample T was less than the 1 °C accuracy of our T measurements.

Conclusion

The solid-liquid phase transitions of stearic acid and palmitic acid were unambiguously observed by STXM with the aid of a variable temperature sample holder device. While being imaged at soft X-ray photon energies, these phase transitions occurred within ±1 °C of their conventionally determined values, even under high dose rate conditions. Therefore, it is inferred that for the conditions investigated, beam-induced heating within the focused spot of the STXM is less than 1 °C. This conclusion does not rely on a direct temperature measurement, but rather is deduced from observations of an equilibrium phase transition which acts as an absolute, sample-dependent thermometer. This indirect method gets around the challenges of directly measuring the temperature of the sample itself within the focal point of the X-ray beam, and separates the issue of beam-induced heating from other effects such as X-ray beam-induced radiation damage.

Acknowledgements

We thank Yosh Kitamura of the McMaster University Engineering Machine Shop for his assistance in fabricating the variable temperature sample holder device, and Dave McLeod for performing the NMR measurement. This research was funded by NSERC, CFI and the Canada Research Chairs program and carried out at beamline 10ID-1 at the CLS and 5.3.2.2 at the ALS. The CLS is supported by NSERC, CIHR, NRC and the University of Saskatchewan. The Advanced Light Source is supported by the Director, Office of Science, Office of Basic Energy Sciences, of the U.S. Department of Energy under Contract No. DE-AC02-05CH11231.

References

1 W. Chao, J. Kim, S. Rekawa, P. Fischer and E. H. Anderson, *Opt. Express*, 2009, **17**, 17669–17677.
2 D. L. Olynick, B. D. Harteneck, E. Veklerov, M. Tendulkar, J. A. Liddle, A. L. D. Kilcoyne and T. Tyliszczak, *J. Vac. Sci. Technol., B*, 2004, **22**, 3186–3190.
3 D. Attwood, in *Soft X-rays and Extreme Ultraviolet Radiation: Principles and Applications*, Cambridge University Press, Cambridge, 1999, ch. 9.
4 C. Jacobsen, S. Williams, E. Anderson, M. T. Browne, C. J. Buckley, D. Kern, J. Kirz, M. Rivers and X. Zhang, *Opt. Commun.*, 1991, **86**, 351–364.
5 A. F. G. Leontowich, T. Tyliszczak and A. P. Hitchcock, *Proc. SPIE*, 2011, **8077**, 80770N-1.
6 J. Thieme, in *X-Ray Microscopy II*, ed. D. Sayre, M. Howells, J. Kirz and H. Rarback, Springer-Verlag, Berlin, 1988, pp. 70–79.
7 T. Warwick, H. Ade, D. Kilcoyne, M. Kritscher, T. Tyliszczak, S. Fakra, A. Hitchcock, P. Hitchcock and H. Padmore, *J. Synchrotron Radiat.*, 2002, **9**, 254–257.
8 A. L. D. Kilcoyne, T. Tyliszczak, W. F. Steele, S. Fakra, P. Hitchcock, K. Franck, E. Anderson, B. Harteneck, E. G. Rightor, G. E. Mitchell, A. P. Hitchcock, L. Yang, T. Warwick and H. Ade, *J. Synchrotron Radiat.*, 2003, **10**, 125–136.
9 T. Tyliszczak, T. Warwick, A. L. D. Kilcoyne, S. Fakra, D. K. Shuh, T. H. Yoon, G. E. Brown, Jr., S. Andrews, V. Chembrolu, J. Strachan and Y. Acremann, *AIP Conf. Proc.*, 2004, **705**, 1356–1359.
10 K. V. Kaznatcheev, Ch. Karunakaran, U. D. Lanke, S. G. Urquhart, M. Obst and A. P. Hitchcock, *Nucl. Instrum. Methods Phys. Res., Sect. A*, 2007, **582**, 96–99.
11 J. Raabe, G. Tzvetkov, U. Flechsig, M. Böge, A. Jaggi, B. Sarafimov, M. G. C. Vernooij, T. Huthwelker, H. Ade, D. Kilcoyne, T. Tyliszczak, R. H. Fink and C. Quitmann, *Rev. Sci. Instrum.*, 2008, **79**, 113704.
12 R. Follath, J. S. Schmidt, M. Weigand and K. Fauth, *AIP Conf. Proc.*, 2010, **1234**, 323–326.
13 M. Born and E. Wolf, in *Principles of Optics*, Cambridge University Press, Cambridge, 7th edn, 1999, pp. 436–446.
14 A. Braun, F. E. Huggins, N. Shah, Y. Chen, S. Wirick, S. B. Mun, C. Jacobsen and G. P. Huffman, *Carbon*, 2005, **43**, 117–124.
15 H. Ade and A. P. Hitchcock, *Polymer*, 2008, **49**, 643–675.
16 A. F. G. Leontowich and A. P. Hitchcock, *Appl. Phys. A: Mater. Sci. Process.*, 2011, **103**, 1–11.
17 J. Wang, C. Morin, L. Li, A. P. Hitchcock, A. Scholl and A. Doran, *J. Electron Spectrosc. Relat. Phenom.*, 2009, **170**, 25–36.
18 J. Fu and S. G. Urquhart, *J. Phys. Chem. A*, 2005, **109**, 11724–11732.
19 H. Hiraoka, *IBM J. Res. Dev.*, 1977, **21**, 121–130.
20 M. C. K. Tinone, K. Tanaka and N. Ueno, *J. Vac. Sci. Technol., A*, 1995, **13**, 1885–1892.
21 A. Cheng and M. Caffrey, *Biophys. J.*, 1996, **70**, 2212–2222.
22 S. V. Postnikov, M. D. Stewart, H. V. Tran, M. A. Nierode, D. R. Medeiros, T. Cao, J. Byers, S. E. Webber and C. G. Wilson, *J. Vac. Sci. Technol., B*, 1999, **17**, 3335–3338.
23 J. Wang, H. D. H. Stöver, A. P. Hitchcock and T. Tyliszczak, *J. Synchrotron Radiat.*, 2007, **14**, 181–190.
24 A. Schöll, R. Fink, E. Umbach, G. E. Mitchell, S. G. Urquhart and H. Ade, *Chem. Phys. Lett.*, 2003, **370**, 834–841.
25 L. Reimer and R. Christenhusz, *Lab. Invest.*, 1965, **14**, 1158–1168.
26 M. Howells, C. Jacobsen and T. Warwick, in *Science of Microscopy*, ed. P. W. Hawkes and J. C. H. Spence, Springer Science + Business Media, New York, 2007, vol. 2, ch. 13.
27 R. C. Moffet, A. V. Tivanski and M. K. Gilles, in *Fundamentals and Aspects of Aerosol Spectroscopy*, ed. R. Signorell and J. P. Reid, CRC Press Taylor & Francis Group, Boca Raton, 2010, ch. 17, pp. 436.
28 R. Dähn, M. Vespa, T. Tyliszczak, E. Wieland and D. K. Shuh, *Environ. Sci. Technol.*, 2011, **45**, 2021–2027.
29 C. Hub, S. Wenzel, J. Raabe, H. Ade and R. H. Fink, *Rev. Sci. Instrum.*, 2010, **81**, 033704.
30 H. Shin, K. Jeong, D. C. Johnson, S. D. Kevan, M. Noh and T. Warwick, *J. Korean Phys. Soc.*, 1997, **30**, 575–579.
31 R. Alberti, A. Longoni, T. Klatka, C. Guazzoni, A. Gianoncelli, D. Bacescu and B. Kaulich, *IEEE Nuclear Science Symposium Conference record*, 2008, **N14-3**, 1564–1566.